

Compression tests of cold-formed channel sections with perforations in the web

Young Bong Kwon ^{1a}, Gap Deuk Kim ^{2b} and In Kyu Kwon ^{*3}

¹ Department of Civil Engineering, Yeungnam University, Gyongsan, 712-749, Korea

² Department of Steel Research, RIST, Incheon, Korea

³ Department of Fire Protection Engineering, Kangwon National University, Samcheok, Korea

(Received March 01, 2013, Revised February 05, 2014, Accepted February 18, 2014)

Abstract. This paper describes a series of compression tests performed on cold-formed steel channel sections with perforations in the web (thermal studs) fabricated from a galvanized steel plate whose thickness ranged from 1.0 mm to 1.6 mm and nominal yield stress was 295 MPa. The structural behavior and performance of thermal studs undergoing local, distortional, or flexural-torsional buckling were investigated experimentally and analytically. The compression tests indicate that the slits in the web had significant negative effects on the buckling and ultimate strength of thin-walled channel section columns. The compressive strength of perforated thermal studs was estimated using equivalent solid channel sections of reduced thickness instead of the studs. The direct strength method, a newly developed and adopted alternative to the effective width method for designing cold-formed steel sections in the AISI Standard S100 (2004) and AS/NZS 4600 (Standard Australia 2005), was calibrated to the test results for its application to cold-formed channel sections with slits in the web. The results verify that the DSM can predict the ultimate strength of channel section columns with slits in the web by substituting equivalent solid sections of reduced thickness for them.

Keywords: thermal studs; slits; perforations; ultimate strength; equivalent thickness; direct strength method

1. Introduction

Cold-formed steel stud sections are typically used as load-bearing members in the wall panel of steel houses and low-rise residential buildings. Stud sections often have perforations in the web for facility use and for heat transfer problems, and these perforations can have negative effects on the structural performance of the sections (Salhab and Wang 2008, Moen and Schafer 2009, Cheng and Li 2012). Because steel is a material of high thermal conductivity, studs have heat-bridging effects between wall panel skins. Thin and long holes (slits) are installed in the web of studs to reduce heat loss from heat bridging and enhance insulating effects. Perforated cold-formed channel

*Corresponding author, Professor, E-mail: kwonik@kangwon.ac.kr

^a Professor, E-mail: ybkwon@ynu.ac.kr

^b Senior Researcher

sections are referred to as thermal studs and these slits in the web of studs may cause significant reduction in the strength and stiffness of studs. However, since studs are used as load-bearing members in the wall panel, they should have sufficient strength and stiffness. This requires an increase in their thickness or the addition of lip and intermediate stiffeners to ensure the sufficient strength and stiffness of thermal studs. In northern European countries, normal thermal studs fabricated by installing slits in the web of cold-formed steel channel sections are commonly used.

The structural behavior and collapse mechanism of thermal studs can become highly complex because of slits in the web, and therefore an accurate estimation of member strength can be difficult. No practical method for predicting compressive and flexural strength has been proposed in existing specifications. Therefore, the finite element analysis or tests should be used to predict the strength capacity of thermal studs. Recently, Hoglund and Burstand (1998) proposed an estimation method for the strength capacity of thermal studs. This method adopted a theoretical method to estimate the structural member capacity. In addition, the effective thickness concept has been proposed to predict the structural capacity of cold-formed steel sections with long holes in the web. In this concept, a solid section of reduced thickness substitutes sections with slits (Davis *et al.* 1997, Kesti 2000, Salhab and Wang 2008). Here the reduction in thickness is determined such that the equivalent solid plate has the same local buckling stress as the perforated plate.

In this paper, a series of thermal studs were tested to their compression failure to investigate their buckling and ultimate strength. Test sections were composed of three types of thermal studs. In addition, numerical analyses of these sections were conducted for comparison purposes. Special shapes of thermal studs with slits in the web were fabricated from a mild steel plate whose thickness was 1.0 mm and nominal yield stress was 295 MPa by cold-rolling and brake-press. The direct strength method (DSM), an alternative to the effective width method for designing cold-formed steel sections adopted recently by AISI Standard (2004) and AS/NZS 4600 (Standard Australia 2005), was calibrated using test results for its application to cold-formed channel sections with slits in the web. Since an estimation of the elastic local and distortional buckling stress of thermal studs was difficult, elastic buckling stress was determined for solid sections substituting for thermal studs by using the effective thickness concept (Salhab and Wang 2008). However, the effective thickness equation was slightly modified to account for the length and pitch of slits, which were neglected in Salhab and Wang's 2008 equations. The strength predicted by the proposed DSM was compared with test results for verification purposes.

2. Material properties and the geometry of test sections

2.1 Material properties

The structural steel grade of test sections was SGC300 (KS D 3506). The minimum specified yield and ultimate stress were 295 MPa and 300 MPa, respectively. Tensile tests of coupons of 1.0 mm in thickness were conducted for flat and corner coupons cut from fabricated sections. All coupons were tested in a 250 kN UTM (Shimazu AUTOGRAPH AG 250kNG) at a displacement rate 0.1 mm/min. The experimental average yield and ultimate stress were 305.0 MPa and 352.0 MPa, respectively, which exceeded the nominal yield and ultimate stress by 3.4% and 17.3%, respectively. The average elongation was 22.5%, slightly exceeding the specified elongation by 18.0%. The yield and ultimate stress of the corner coupon were slightly higher than those of flat coupons because of the cold working of brake-pressed corners.

2.2 Section geometry

Three basic types of thermal studs were chosen for compression tests. Test sections were categorized in three groups according to their section geometry. Figs. 1(a)-(c) show their cross-sectional geometry. The typical lipped channel section 150SL10 (web 150 mm × flange 40 mm × lip 12 mm × thickness 1.0 mm) is widely used for wall panel studs in steel houses and residential buildings in Korea. The overall shape of Type A and Type B section was the same as the plain 150SL10 section except for perforations in the web. Increasing the thickness of sections may be the simplest way to compensate for reductions in strength from perforations. Therefore, the thickness of Type A and Type B sections chosen for the tests ranged from 1.0 mm to 1.6 mm. The slits of Type A and Type B studs were made by piercing. The Type A section was a plain lipped channel section with six perforation lines at the web center. The Type B section was also a plain lipped channel section with large holes at the center for the facility and three perforation lines on each side of central holes in the web. The Type C section was a special lipped channel section whose web was folded to compensate for reductions in strength from perforations made for reducing heat loss from heat-bridge effects. The overall width of the Type C section was the same as that of other test sections. The Type C section had two or three slit lines in each flat area of the folded web, as shown in Fig. 1(c). The slits of the Type C section of 1.0 mm in thickness were made by burring.

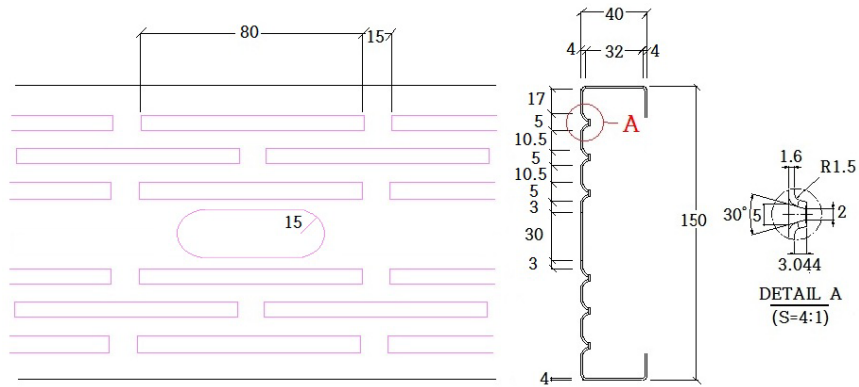
Longitudinal solid distances between adjacent slits were 15 mm for Type A and Type B sections and 20 mm for the Type C section. Transverse solid distances between adjacent slits were 5 mm for Type A and Type B sections and 3 mm for the Type C section. Clear widths of slits were 2 mm for Type A and Type B sections and 3 mm for Type C section, and the slit length was normally 80 mm for all types of sections. However, for special Type C sections, the slit length was 200 mm, and the solid length was 5 mm. Overall lengths of test sections ranged from 400 mm to 2,000 mm.

Main factors in the compression test were the shape of sections, the length of slits, the arrangement of slits, and the solid distance between adjacent slits. Test sections were labeled to indicate section type, the slit length, the solid distance between adjacent slits in the longitudinal direction, and the total length. For example, in the label A-80-15-1.0-420, A refers to Type A with two slit lines arranged; 80, to the slit length in millimeters; 15, to the solid distance between adjacent slits in the longitudinal direction in millimeters; 1.0, to the thickness in millimeters; and 420, to the overall length in millimeters.

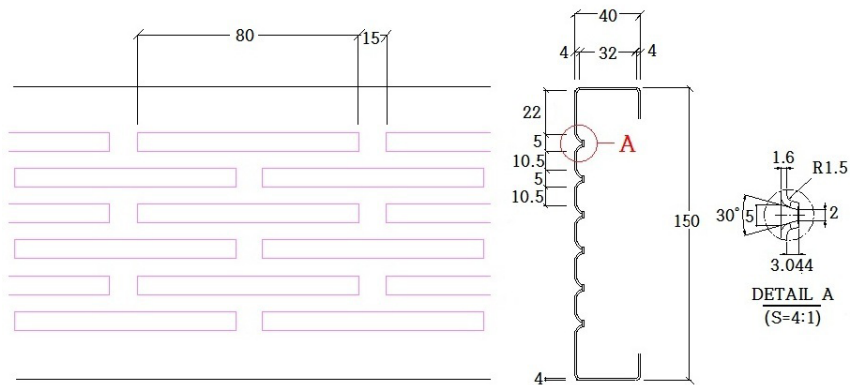
Table 1 summarizes the properties of test sections. The properties of Type A and Type B cross sections were computed based on sections of 1.0 mm in thickness. The moment of inertia of Type

Table 1 Test section properties

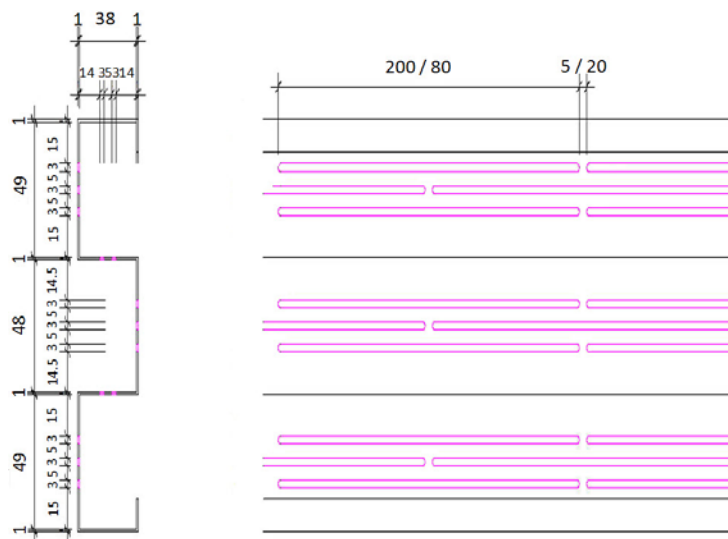
Specimens	Slit arrangement	Thickness (mm)	Net area (mm ²)	Gross area (mm ²)	Moment of inertia (mm ⁴)
Type-A	2 × 3 lines	1.0 (1.2, 1.4, 1.6)	238.0	250.0	828040.0
Type-B	6 lines	1.0 (1.2, 1.4, 1.6)	238.0	250.0	832059.0
Type-C	3 × 3 + 2 × 2 lines	1.0	287.0	328.0	787222.0
150SL10	no slits	1.0	250.0	250.0	845514.0



(a) Type A section



(b) Type B section



(c) Type C section

Fig. 1 Geometry of test sections

A, Type B, and Type C sections was calculated based on a net area of test sections of 1.0 mm in thickness. The properties of the Type A section were computed by ignoring the utility hole at the web center. The properties of the plain channel section 150SL10, which is a normal lipped channel section of 150 mm in web depth, 40 mm in flange width and 12 mm in lip width, were included in Table 1 for comparison purposes.

3. Buckling analysis of thermal studs

The commercial FE analysis program LUSAS (ver. 14.3) was used for the buckling analysis of thermal studs to investigate the effects of the main test factors (e.g., the distance and length of slits) and select the optimum geometry of sections for the compression test. An eight-node shell element was selected for numerical modeling. Slits were assumed to be rectangular for modeling convenience. Both section ends were assumed to be the same fixed boundary conditions as those in compression test. The rotation and translation in the x- and y-directions were assumed to be restrained, but the translation in the z-direction was not. The uniform compression load was applied at the upper end of the thermal stud section. For those slits at section ends, virtual elements were added for uniform compression. Fig. 2(a) shows the results of numerical modeling. The overall lengths of sections in the numerical analysis were determined to be 410 mm, 820 mm, 1,140 mm, 1,440 mm, 2,000 mm, and 2,840 mm for the Type C section for modeling convenience. However, the overall lengths were slightly different for Type A and Type B sections because of slit lengths in numerical modeling. The slit (neglecting rims) was assumed to be rectangular.

Figs. 2(a) and (b) show the typical local and distortional buckling modes of the Type C section obtained by the FE analysis. The typical distortional buckling mode in Fig. 2(a) was interacted with the local buckling mode in the web. The distortional buckling of long half-waves in flanges was interacted with the local buckling of short half-waves in the web. As shown in Fig. 2(b), the local buckling mode of the Type C section was quite different from the conventional local buckling mode of plain lipped channel sections. In the local buckling mode of the Type C section, the solid strips between slits in the web buckled locally. However, the local buckling modes of Type A and Type B sections were simple and similar to the conventional local buckling mode of plain lipped channel sections regardless of the overall length.

The three lowest buckling stress values for the three types of thermal studs and the plain lipped channel section 150SL10, which is commonly used as a load-bearing member in steel houses in Korea, are summarized in Tables 2A-D for comparison purposes. Here L, D, and F indicate local buckling, distortional buckling, and flexural/flexural-torsional buckling, respectively. The value in parentheses (e.g., L(4)) indicates the number of buckle half-waves. As shown in Tables 2A and B, despite the large facility holes at 500 mm intervals in the web, the local buckling stress of the Type A thermal stud was slightly lower than that of the Type B thermal stud. This may be largely due to the concentration of holes at the web center for the Type B section. As shown in Tables 2A-C, critical buckling was local buckling for all three types of sections except for the Type C section C-80-20-1.0-2835. The critical local buckling stress values for all sections except for those 300 mm in length were generally consistent because the effect of the boundary condition decreased according to an increase in the total length. The magnitude of the local buckling stress of Type A and Type B sections was much lower than that of the plain lipped channel section 150SL10 of the same thickness because of perforations. The local buckling stress of Type A and Type B sections of 1.4 mm in thickness was quite similar to that of the 150SL10 section of 1.0 mm in thickness.

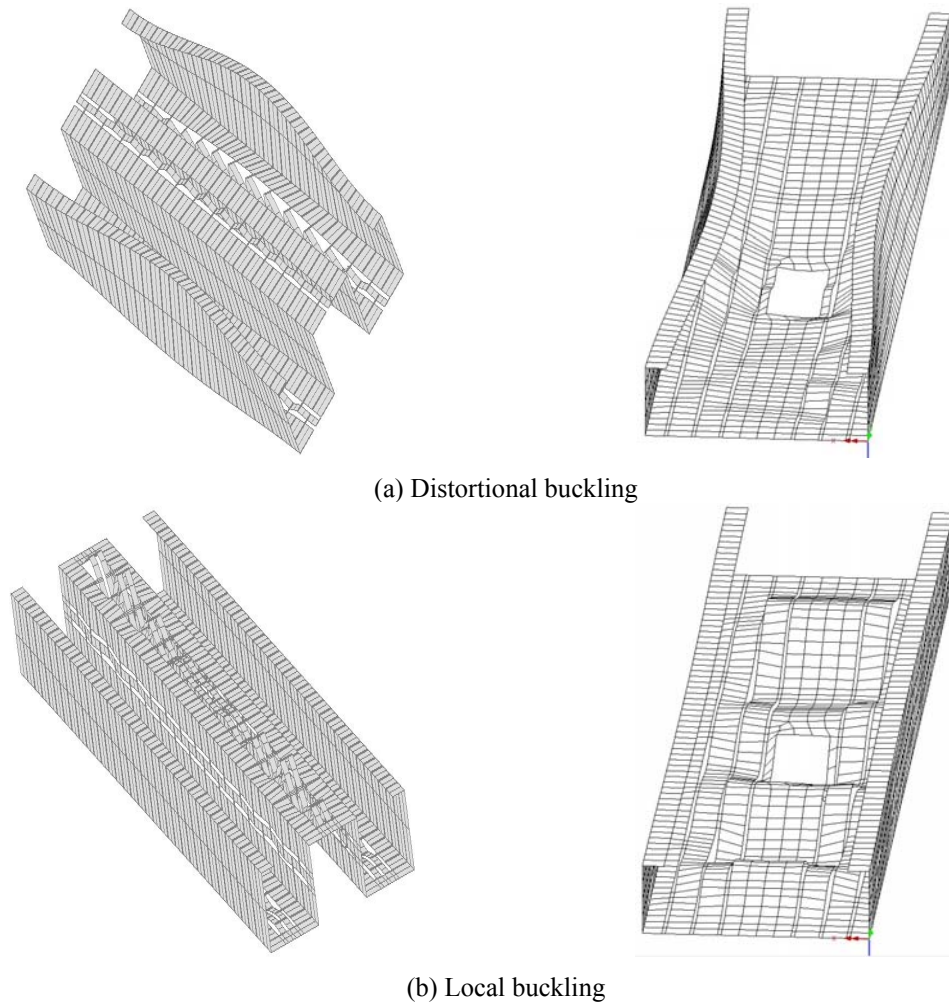


Fig. 2 Buckled shape of Type-A and Type-C sections

Table 2A Buckling stress of Type A thermal studs

Sections	Buckling stress and mode					
	1st		2nd		3rd	
	Stress (MPa)	Mode*	Stress (MPa)	Mode	Stress (MPa)	Mode
A-80-15-1.0-300	30.4	L(2)	36.6	L(3)	46.0	L(3)
A-80-15-1.0-585	27.2	L(5)	28.7	L(4)	33.1	L(5)
A-80-15-1.0-775	26.6	L(5)	27.5	L(6)	29.0	L(7)
A-80-15-1.0-1155	26.5	L(9)	26.8	L(9)	27.8	L(11)
A-80-15-1.0-1440	26.4	L(11)	26.8	L(11)	27.3	L(12)
A-80-15-1.0-2010	26.1	L(13)	26.3	L(15)	26.8	L(15)

Mode*: L: local buckling; F: flexural/flexural-torsional buckling

Table 2B Buckling stress of Type B thermal studs

Sections	Buckling stress and mode					
	1st		2nd		3rd	
	Stress (MPa)	Mode*	Stress (MPa)	Mode	Stress (MPa)	Mode
B-80-15-1.0-300	34.1	L(2)	37.4	L(3)	55.5	L(3)
B-80-15-1.0-585	30.5	L(4)	30.8	L(5)	35.7	L(5)
B-80-15-1.0-775	30.0	L(6)	30.1	L(6)	32.6	L(7)
B-80-15-1.0-1155	29.6	L(9)	29.6	L(9)	30.7	L(10)
B-80-15-1.0-1440	29.4	L(11)	29.5	L(12)	30.2	L(12)
B-80-15-1.0-2010	29.3	L(16)	29.3	L(16)	29.8	L(17)

Table 2C Buckling stress of Type C thermal studs

Sections	Buckling stress and mode					
	1st		2nd		3rd	
	Stress (MPa)	Mode*	Stress (MPa)	Mode	Stress (MPa)	Mode
C-80-20-1.0-410	77.12	L(4)	77.34	L(4)	78.51	L(4)
C-80-20-1.0-820	77.15	L(9)	77.15	L(9)	78.48	L(9)
C-80-20-1.0-1130	77.15	L(11)	77.15	L(12)	78.50	L(12)
C-80-20-1.0-1435	77.16	L(14)	77.16	L(14)	78.52	L(15)
C-80-20-1.0-1995	77.18	L(20)	77.18	L(21)	78.52	L(21)
C-80-20-1.0-2835	63.06	F	77.20	L(29)	77.20	L(30)

Table 2D Buckling stress of 150SL10 sections

Sections	Buckling stress and mode					
	1st		2nd		3rd	
	Stress (MPa)	Mode*	Stress (MPa)	Mode	Stress (MPa)	Mode
150SL10-300	59.2	L(3)	60.1	L(4)	80.0	L(5)
150SL10-585	53.6	L(7)	54.3	L(6)	59.4	L(8)
150SL10-775	52.9	L(9)	53.0	L(8)	56.3	L(10)
150SL10-1155	52.3	L(12)	52.3	L(12)	53.8	L(13)
150SL10-1440	52.1	L(17)	52.1	L(18)	53.2	L(19)
150SL10-2010	51.9	L(25)	52.0	L(24)	52.5	L(26)

However, the local buckling stress of the Type C section was much higher than that of the 150SL10 section of the same thickness because of an increase in stiffness by the folded web.

If either the distortional or flexural-torsional buckling stress is not much higher than the local buckling stress, then an interaction between local buckling and distortional buckling or flexural-torsional buckling is likely to occur for those sections whose local critical buckling modes are local. There was little difference between local and distortional buckling stress for test thermal studs of intermediate length, indicating some interaction between local buckling and distortional

Table 3A Local buckling stress of Type C thermal studs with varying slit lengths (MPa)

Sections	Slit length (mm)			
	80	100	150	200
C-[]-5-400	65.2	43.1	21.7	13.4
C-[]-5-840	64.7	41.7	20.8	12.5
C-[]-5-1140	64.7	41.5	20.7	12.4
C-[]-5-1440	64.7	41.3	20.6	12.3
C-[]-5-2000	64.6	41.3	20.5	12.2
C-[]-5-2840	64.6	41.3	20.5	12.2

Table 3B Local buckling stress of Type C thermal studs with varying solid lengths (MPa)

Sections	Solid distance (mm)				
	5	10	20	30	40
C-80-[]-400	65.2	71.9	79.7	80.5	81.2
C-80-[]-840	64.7	71.7	79.3	80.0	80.8
C-80-[]-1140	64.7	71.7	79.3	80.0	80.8
C-80-[]-1440	64.7	71.6	79.3	80.0	80.8
C-80-[]-2000	64.6	71.6	79.3	80.0	80.8
C-[]-5-2840	64.6	71.6	79.3	80.0	80.8

buckling during the test of those sections.

For an analysis of the effects of the slit length and the solid distance in the longitudinal direction on the local buckling stress of thermal studs, the buckling stress of Type C thermal studs of varying slit lengths and clear slit distances is summarized in Tables 3A and B, respectively. As shown in Table 3A, an increase in the slit length slightly reduced the elastic local buckling stress of thermal studs, as indicated in Wang and Salhab (2009). This decreasing trend was nearly linear according to an increase in the slit length. An increase up to 20 mm in the solid distance between adjacent slits in the longitudinal direction slightly increased local buckling stress. However, an increase in the clear slit distance beyond 20 mm had little effect on local buckling stress. The local buckling mode in Fig. 2(b) was different from the conventional local buckling of plain sections without perforations, indicating that the slit length had a slightly greater effect on the local buckling stress of solid parts between slits than the slit distance in the longitudinal direction.

4. Compression tests

4.1 General

A series of compression tests was conducted to examine the structural behavior and performance of thermal studs. A total of 38 intermediate and long studs for Type A, Type B, and Type C sections were tested under axial compressive load to failure. The steel grade of test sections was SGC300 galvanized steel to KS D3506 (2006), whose nominal yield stress and

ultimate tensile stress were 295 MPa and 300 MPa, respectively. The test section length determined through the FE analysis ranged from approximately 400 mm to 2,000 mm.

A single symmetric section may induce a shift in the line of axial force after local and distortional buckling if it is loaded between pinned ends. A shift in the centroid of sections has a significant effect on the ultimate strength of columns. To avoid this problem, fixed end boundary conditions were used in tests using a specially designed capping system made of unsaturated polyester resin (Kwon *et al.*, 2009). Fig. 3 shows the procedure of capping on stud ends. The wooden frame was fabricated first, and a thin steel plate was installed at the bottom of the wooden frame. Then the specimen was set upright at the center of the wooden frame, and finally the unsaturated polyester resin mixed with a hardening material was poured into the wooden frame up to 40 mm in thickness. The wooden frame was removed at least two weeks after the casting of the resin material to acquire required strength. Compression tests were conducted after removing the wooden frame. The unsaturated polyester resin used as the capping material had several advantages over pattern stone or cement mortar, including rapid hardening, high strength, and high



Fig. 3 Capping on stud ends



(a) 250 kN UTM



(b) 1000 kN UTM

Fig. 4 Compression test set up

energy absorption capacity. It was not difficult to center the column at the loading plate of the UTM because the capping material was semi-transparent, as shown in Fig. 3. The resin capping effectively prevented both the local failure and warping of test section ends.

A concentric pseudo-static compression test was conducted using 250 kN and 1,000 kN Shimadzu testing machines according to the length of test sections. Figs. 4(a) and (b) show the typical compression test configurations for specimens. The downward loading was controlled by the displacement control method with the loading velocity of 0.01 mm/min. The vertical displacement was obtained from the machine directly, and the horizontal displacement was measured by a maximum of six displacement transducers (LVDTs) attached at the center and quarter points along test specimens, as shown in Figs. 4(a) and (b). Two LVDTs were attached at the center of each folded web, and one LVDT was attached at the joint line between the flange and the lip stiffener, as shown Fig. 4(a). Because the height limit of specimens was 1,500 mm for the 250 kN testing machine, a 1,000 kN machine was used for sections whose overall length exceeded 1,500 mm. The test load capacity was adjusted to 250 kN for more accurate test results because of the expected magnitude of the maximum load range.

4.2 Test results

After the initial take-up, the axial shortening of sections was increased linearly according to the load increment before local or distortional buckling. For most test sections, when the load was increased, the nonconventional local buckling of perforated parts occurred first (as expected), and a significant post-buckling strength was observed before the commencement of distortional buckling. Finally there was a buckling interaction between local and distortional buckling, and the test section collapsed mainly in the distortional mode, as shown in Figs. 5(a)-(h). Based on the test results, all the test specimens showed similar structural behaviors regardless of their shape and length. The solid parts between slits in the web of specimens buckled in a local mode, as shown in Fig. 5(a), during the stage of very low loading. The local buckling mode was quite different from the conventional local buckling mode, which occurred in channel sections without slits. When the load was increased, all the test specimens showed a distortional or flexural-torsional buckling behavior and finally failed, as shown in Figs. 5(b) and (c). After the occurrence of distortional buckling, a significant post-buckling strength reserve was displayed. The main reason for the failure of the test specimens was the growth of deformations from distortional buckling. Some specimens of 1,435 mm in length displayed a flexural-torsional buckling mode because of initial imperfections. A decrease in stiffness from the occurrence of local buckling was negligible, but distortional buckling had considerable influence on the stiffness and strength of specimens. Distortional buckling had some post-buckling strength reserve as well as conventional plain sections.

Figs. 6(a) and (b) show the axial load versus displacement curves for test sections. As shown in Fig. 6(a), those specimens of 200 mm to 1,130 mm in length showed a significant post-local-buckling strength and a sharp drop of loading after the peak load. However, those exceeding 1,435 mm showed flexural-torsional buckling and a gradual decrease in loading after the maximum load. For these sections, fairly large axial displacements were observed at the point of failure. As shown in Fig. 6(b), all the specimens with slits of 80 mm in length showed similar load versus axial shortening. The deterioration of stiffness from local buckling was not detected on load versus displacement curves. However, after post-local-buckling was displayed, there was distortional buckling in most test sections. Most test sections showed a slight post-buckling strength in the

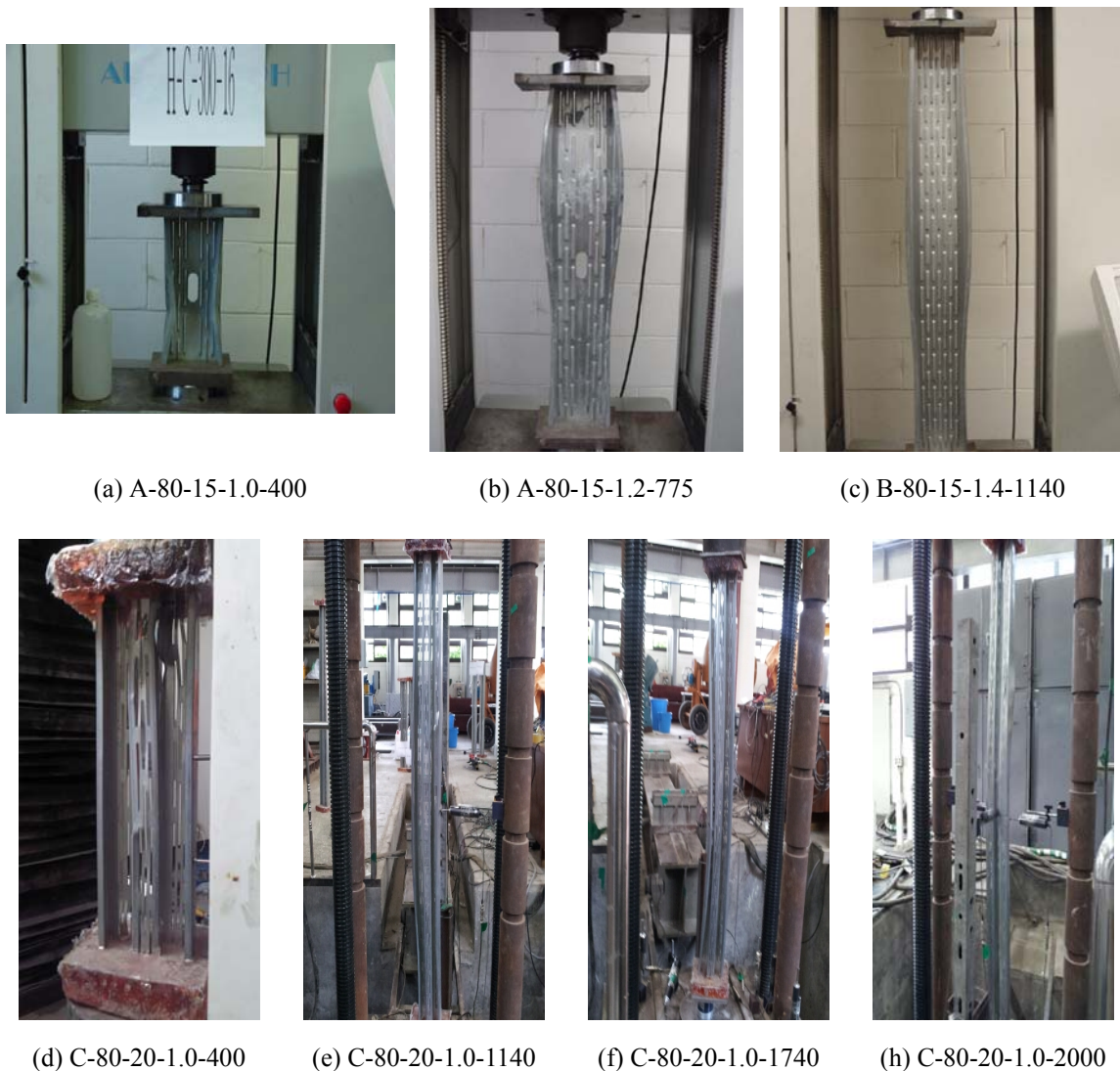
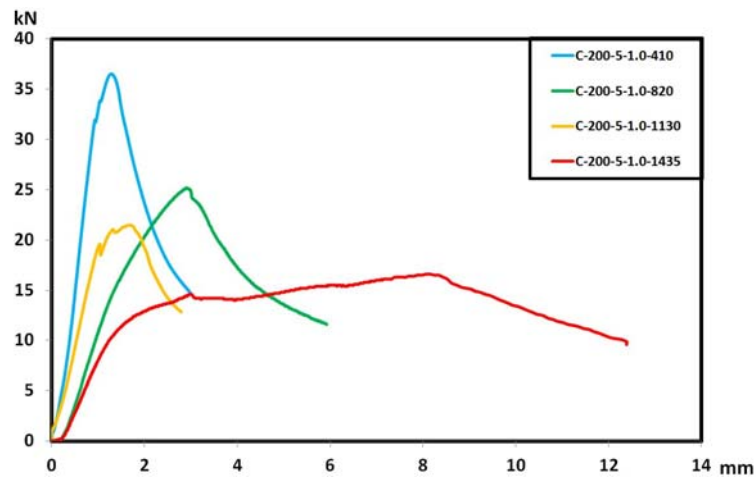


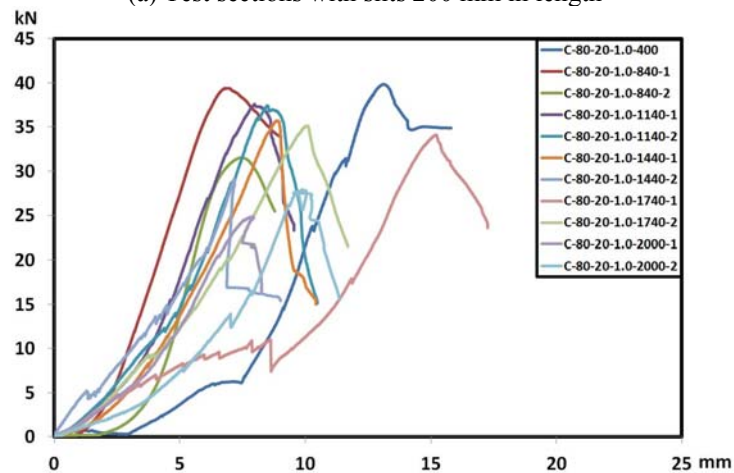
Fig. 5 Failure modes of thermal studs

distortional buckling mode before the maximum load and displayed a sudden drop in the load after the maximum load before their final failure. Resin used in capping of the column end did not failed to the final collapse of columns and restrained the warping deformation effectively during testing as expected.

Because Type A, Type B, and Type C sections of intermediate or long length buckled in the distortional or overall mode, which was interacted with the local buckling of short half-waves, the load-bearing capacity of thermal studs was significantly affected by the stud ends condition. The fixed end boundary condition (Fig. 3) shortened the half-wavelength of distortional buckling and flexural-torsional buckling by half and consequently led to significant increases in distortional or



(a) Test sections with slits 200 mm in length



(b) Test sections with slits 80mm in length

Fig. 6 Axial load vs. shortening curves

flexural-torsional buckling stress. In practice, thermal studs in load-bearing wall panels are generally fabricated by attaching plaster boards at both flanges with screws, and therefore distortional buckling can be effectively restrained. However, the restraining effect on flexural-torsional buckling about the major axis is much weaker than that on distortional buckling. Consequently, the ultimate strength of thermal studs may be determined by local and post-local buckling strength and overall, not distortional, buckling strength.

Table 5 summarizes the local, distortional, or flexural-torsional buckling and maximum loads based on the tests. In all cases, the maximum stress was less than half of yield stress ($F_y/2$). This suggests that local, distortional, and flexural-torsional buckling stress may be elastic. Because there were only subtle changes in overall flexural stiffness from local buckling, the commencement of local buckling was determined by a hand touch during testing and by

examining changes in the slope on load-horizontal displacement curves or load-axial shortening curves. Because it was difficult to determine distortional or flexural-torsional buckling stress for columns tested, this stress was taken as that where the deterioration of stiffness on load versus displacement curves commenced. Distortional buckling stress was determined by examining changes in the slope of load versus displacement curves. The intersection between the fitted line and stress axis was assumed to be experimental buckling stress (Venkataramaiah and Roorda 1982). As shown in Table 5, local buckling loads were much lower than maximum loads. The difference between the local buckling stress and the maximum stress in Table 5 indicates a

Table 5 Experimental buckling and maximum loads of specimens

Specimens	Local buckling loads (kN)	Distortional or flexural – torsional buckling loads (kN)	Maximum loads (kN)	Maximum stress (MPa)
A-80-15-1.0-300	7.8	-	38.7	154.8
A-80-15-1.0-585	7.4	-	36.8	147.2
A-80-15-1.0-775	5.6	25.9(D)	31.9	127.6
A-80-15-1.0-1155	6.7	23.3(D)	27.4	109.6
A-80-15-1.0-1440	6.5	16.9(D)	19.5	78.0
A-80-15-1.0-2010	6.6	16.7(D)	20.1	80.4
B-80-15-1.0-300	6.9	-	34.5	138.0
B-80-15-1.0-585	6.3	-	38.2	152.8
B-80-15-1.0-775	5.9	27.4(D)	32.1	128.4
B-80-15-1.0-1155	6.8	25.3(D)	28.4	113.6
B-80-15-1.0-1440	6.1	20.1(D)	22.1	88.4
B-80-15-1.0-2010	6.0	19.2(D)	21.8	87.2
C-200-5-1.0-410	5.1	33.2(D)	36.5	111.3
C-200-5-1.0-820	4.5	15.3(D)	25.2	76.8
C-200-5-1.0-1130	4.2	12.9(D)	20.1	61.3
C-200-5-1.0-1435	4.9	11.2(D)	16.6	50.6
C-80-20-1.0-400	25.2	36.5(D)	39.0	118.9
C-80-20-1.0-840-1	23.2	35.0(D)	38.4	117.1
C-80-20-1.0-840-2	23.8	26.5(D)	30.9	94.2
C-80-20-1.0-1140-1	23.0	32.5(D)	36.8	122.0
C-80-20-1.0-1140-2	21.0	35.5(D)	36.7	111.9
C-80-20-1.0-1440-1	22.5	34.0(D)	35.0	106.7
C-80-20-1.0-1440-2	22.8	27.7(D)	28.5	86.9
C-80-20-1.0-1740-1	19.8	33.2(D)	33.4	101.8
C-80-20-1.0-1740-2	18.0	34.4(D)	34.4	104.9
C-80-20-1.0-2000-1	20.0	24.0(FT)	24.3	74.1
C-80-20-1.0-2000-2	21.2	27.2(FT)	27.3	83.2

D: distortional buckling; FT: flexural-torsional buckling

significant post-buckling strength after local buckling for most test sections. Local buckling and interactions with distortional or flexural-torsional buckling had negative effects on the ultimate strength of all the specimens. These results provide clear evidence that perforations in the web had significant negative effects on the local buckling stress and the ultimate strength of thermal studs. Maximum stress is obtained from the maximum load divided by the gross area.

5. Section strength estimation method

5.1 Equivalent thickness

The design strength of thermal studs with slits cannot be estimated directly based on current specifications such as the AISI Standard (2012), Eurocode 3 (2001), and AS/NZS 4600 (Standard Australia 2005). Davis *et al.* (1997), Kesti (2000), and Salhab and Wang 2008 proposed the concept of equivalent thickness in which the plain solid stud of reduced thickness substitutes the thermal stud with slits in the web. The design strength of thermal studs can be substituted by the strength of solid studs of equivalent thickness. Salhab and Wang 2008 equation for the equivalent thickness of usual cold-formed sections with slits ($Y > 0.00133$) can be expressed as

$$t_{eq} = \sqrt[3]{C_1 + C_2 Y} \cdot t \quad (Y \geq 0.00133) \quad (1)$$

where

$$C_1 = 0.608 - 1.7t/b \quad (2)$$

$$C_2 = 70.256t/b - 18.33 \quad (3)$$

$$Y = (p_b/b)^2 (w_s/w_p)^{0.5} \quad (4)$$

p_b : total width of slits

b : plate width

t : plate thickness

w_s : transverse distance between slits

w_p : distance between exterior slits

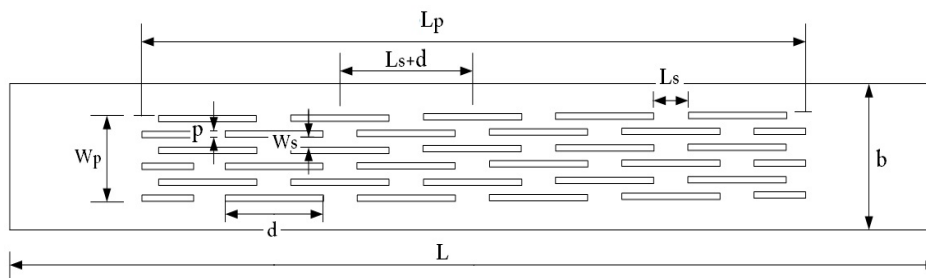


Fig. 7 Equivalent thickness parameters for thermal studs (Salhab and Wang 2008)

These equations were proposed on the assumption that the length of single slit ranges from 65 mm to 85 mm and that this length had little effect on the local buckling stress of thermal studs. As clearly shown in Table 3B, the solid length in the longitudinal direction had little effect on local buckling stress. However, the effect of the slit length exceeding 85 mm on local buckling stress was not negligible, as shown in Table 3A. For an analysis of the relationship between the slit length and equivalent thickness, Fig. 8 shows the square root of the ratio of the local buckling stress of thermal stud to that of the plain section versus the slit length. The relationship between the slit length and the square root of local buckling stress can be assumed as linear. An increase in the slit length had a significant negative effect on local buckling stress. This suggests that the effects of the slit length should not be neglected in estimating the equivalent thickness of thermal studs with longer slits than 85 mm. For thermal studs with long slits, the equation for sections with slit lengths from 65 mm to 85 mm (Wang and Salhab 2009) should be modified to account for the effects of long slit lengths on the thickness reduction factor.

The ratio of equivalent thickness to the original thermal stud thickness can be assumed to have a linear relationship with the ratio of the buckling stress of the equivalent solid stud to that of the thermal stud. To account for the effects of the slit length in the longitudinal direction on the thickness reduction factor in a simple manner, the equation for equivalent thickness can be modified as

$$t_{eq} = C_3 \sqrt{C_1 + C_2 Y} \cdot t \quad (Y \geq 0.00133) \tag{5}$$

where $C_3 = -0.0039d + 1.315 (\leq 1.0)$ and $d =$ slit length.

The modified formula uses the square root instead of its cubic root and includes the factor C_3 to account for the effect of the slit length on the buckling stress of thermal studs. Salmi (1998) and Kesti (2000) proposed the use of the square root of local buckling stress ratio. The equivalent thickness computed by the modified formula for the C-80-20-1.0 section was 0.531 mm for the web and 0.553 mm for the intermediate stiffener; that for the C-200-5-1.0 section was 0.293 mm

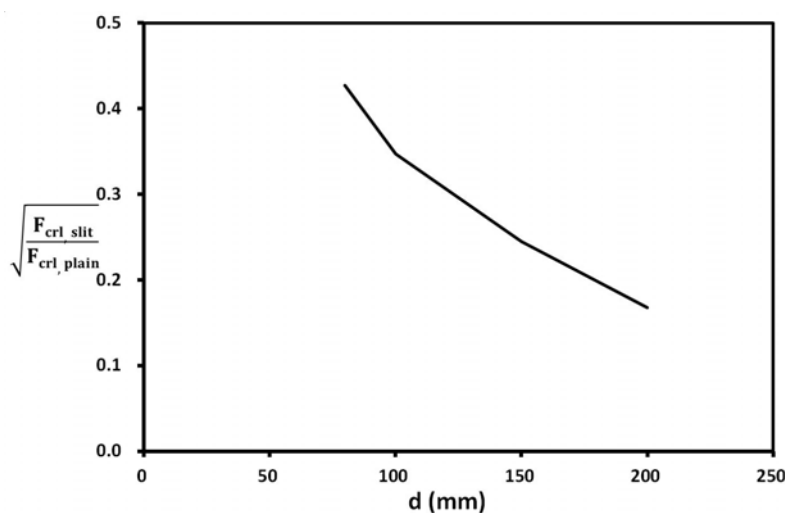


Fig. 8 Effects of the slit length on local buckling stress

for the web and 0.301 mm for the stiffener; that for the A-80-15-1.0 section was 0.755 mm; and that for the B-80-15-1.0 section was 0.754 mm.

Although the modeling of thermal studs is usually complicated because of perforations, if an accurate FE analysis is available for thermal studs, then a more convenient method for computing the thickness reduction factor is to use FE analysis results directly (Salmi 1998). The thickness reduction factor for the section was calculated by the following equation based on the direct application of FE buckling analysis results

$$k_{red} = t_e/t = \sqrt{F_{crl,slit}/F_{crl,plain}} \quad (6)$$

where $F_{crl,slit}$ is the elastic local buckling stress of thermal studs with slits in the web and $F_{crl,plain}$ is that of solid studs with no perforations, which can be computed through the FE analysis. When the FE analysis is available, Eq. (6) may be convenient to compute equivalent thickness. However, because the accurate FE modeling of thermal studs is generally not simple, reduced thickness concept could conveniently be applied to the perforated web of thermal studs.

5.2 Design strength-direct strength method

The compressive strength of equivalent solid sections with reduced thickness in the web can be computed by the direct strength method, a method developed by Schafer and Pekoz (1998) and recently adopted by AISI Standard Supplementary 1 (AISI 2004) and AS/NZS 4600 (Standard Australia 2005). This method has been verified to be as good as or slightly better than the effective width method (Shafer 2008). The method to overcome the limitations of the effective width method, including the accurate computation of the effective width and the consideration of elements interacted in isolation as the shape of cold-formed steel sections become more complex with additional edges and intermediate stiffeners. Previous studies have examined the interaction between local or distortional buckling and overall buckling for cold-formed steel sections and proposed simple design formulas. The method makes direct use of the gross section and strength formula accounting for the interaction between elastic local or distortional buckling stress, and overall buckling stress. Recently, Kwon *et al.* (2009) proposed a strength formula for the direct strength method that accounts for the interaction between local and distortional buckling stress.

The direct strength formula adopted by the AISI Standard (2004) and AS/NZS 4600 (Standard Australia 2005), which accounts for the interaction between local buckling and overall buckling for cold-formed steel sections, is

$$P_{nl} = P_{ne} \quad \text{for } \lambda_l \leq 0.776 \quad (7a)$$

$$P_{nl} = \left(1 - 0.15 \left(\frac{P_{crl}}{P_{ne}} \right)^{0.4} \right) \left(\frac{P_{crl}}{P_{ne}} \right)^{0.4} P_{ne} \quad \text{for } \lambda_l > 0.776 \quad (7b)$$

where $\lambda_l = \sqrt{P_{ne}/P_{crl}}$; P_{nl} = limiting stress accounting for local and overall buckling; P_{crl} ($= F_{crl} \cdot A$) = the elastic local buckling load; A = gross section area; and P_{ne} ($= F_{ne} \cdot A$) = overall column strength based on the overall failure mode determined from the minimum of elastic flexural, torsional, and flexural-torsional buckling stress. Overall column strength F_{ne} can be calculated from Eqs. (C4-2) and (C4-3) in the AISI Standard (2007), and elastic local buckling stress F_{crl} can

be computed by the rigorous finite element method (FEM) or the finite strip method (FSM).

Because Type A and Type B sections shorter than 1000 mm failed in the local buckling mode, the nominal axial strength P_{nl} in Eqs. (7a) and (7b) was compared with test results for those sections in Fig. 9. The strength curve conservatively predicted the ultimate strength of stub columns that failed in the local buckling mode. This suggests that the formula for local buckling strength can be used for predicting the ultimate strength of thermal studs that are substituted by solid sections of reduced thickness which can be computed by Eq. (5).

Previously, strength formulae that account for the distortional buckling of cold-formed sections were proposed and have been adopted by the AISI STANDARD (2004) and AS/NZS 4600(2005). The distortional buckling limiting strength is given by

$$P_{nd} = P_y \quad \text{for } \lambda_d \leq 0.561 \tag{8a}$$

$$P_{nd} = P_y \left[1 - 0.25 \left(\frac{P_{crd}}{P_y} \right)^{0.6} \right] \left(\frac{P_{crd}}{P_y} \right)^{0.6} \quad \text{for } \lambda_d > 0.561 \tag{8b}$$

where $\lambda_d = \sqrt{P_y / P_{crd}}$; P_{crd} ($= F_{crd} \cdot A$) = elastic distortional buckling load; and P_y ($= F_y \cdot A$) = nominal yield load. Elastic distortional buckling stress F_{crd} should be computed by the FEM or the spline finite strip method (SFSM), which can account for real end boundary conditions instead of simple ones.

Since most of the test sections failed in the distortional buckling mode, the formula for distortional strength was compared with test results showing failures in the distortional buckling mode (Fig. 10). The strength predicted by Eqs. (8a) and (8b) was too unconservative in comparison with test results because the distortional buckling strength curve from these two equations cannot

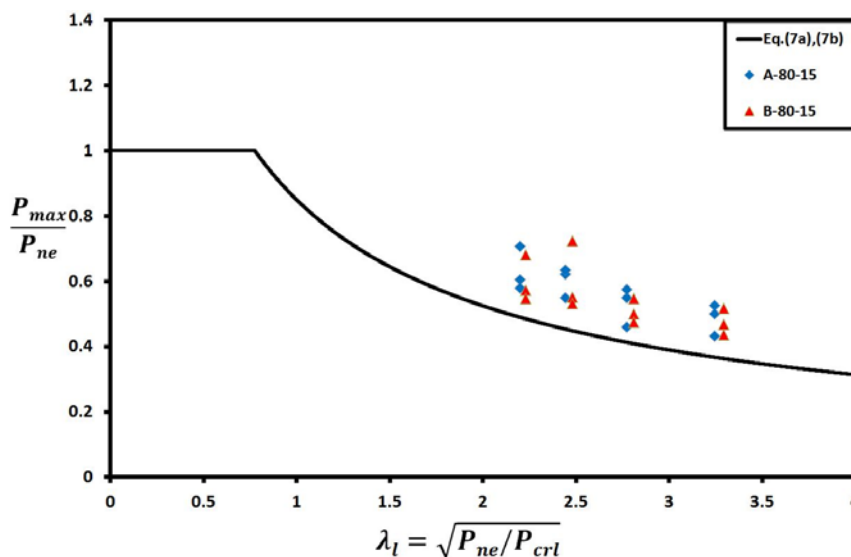


Fig. 9 Comparison of local buckling strength curve and test results

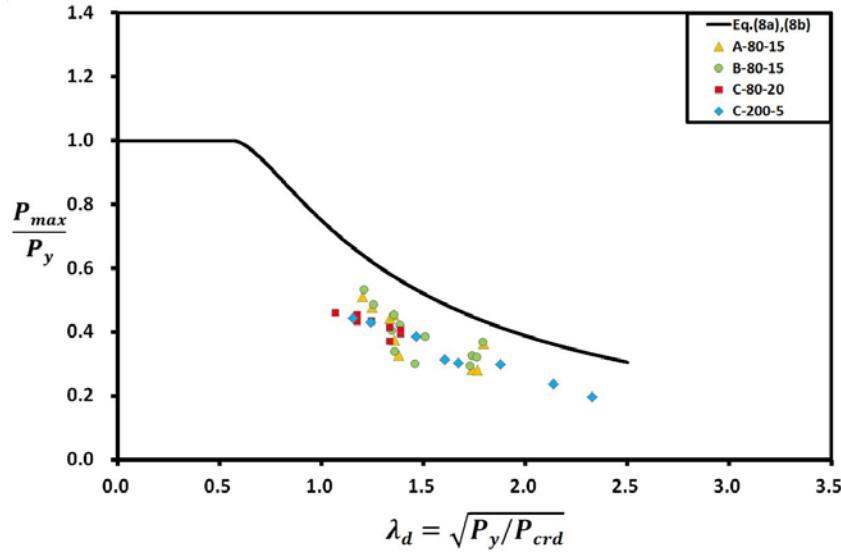


Fig. 10 Comparison of distortional buckling strength curve and test results

account for the interaction between local buckling and distortional buckling and the negative effect of local buckling on column strength. This suggests that the formula for distortional buckling strength is not suitable for predicting the ultimate strength of thermal studs that fail in the mixed mode of distortional and local buckling.

The strength formulae should account for the interaction between local buckling and distortional buckling to accurately predict the ultimate strength of thermal studs with interactions between local buckling and distortional buckling. Kwon *et al.* (2009) proposed a strength formula accounting for the interaction between local buckling and distortional buckling of cold-formed sections

$$P_{nld} = P_{kh} \quad \text{for } \lambda_{dl} \leq 0.667 \tag{9a}$$

$$P_{nld} = P_{kh} \left[1 - 0.2 \left(\frac{P_{crd}}{P_{kh}} \right)^{0.4} \right] \left(\frac{P_{crd}}{P_{kh}} \right)^{0.4} \quad \text{for } \lambda_{dl} > 0.667 \tag{9b}$$

where $\lambda_{dl} = \sqrt{P_{kh} / P_{crd}}$; P_{nld} = design compressive load; and P_{kh} ($= F_{kh} \cdot A$) = distortional buckling strength computed by Eqs. (10a) and (1b). The distortional buckling limiting stress F_{kh} proposed by Kwon and Hancock (1992) is

$$F_{kh} = F_y \quad \text{for } \lambda_{nd} \leq 0.561 \tag{10a}$$

$$F_{kh} = F_y \left[1 - 0.25 \left(\frac{F_{crd}}{F_y} \right)^{0.6} \right] \left(\frac{F_{crd}}{F_y} \right)^{0.6} \quad \text{for } \lambda_{nd} > 0.561 \tag{10b}$$

where $\lambda_{nd} = \sqrt{F_y / F_{crd}}$; F_{crd} = elastic distortional buckling stress; and F_y = nominal yield stress.

The design strength of thermal studs predicted by the strength formula for the interaction

between local buckling and distortional buckling in Eqs. (9a) and (9b) was compared with the test results (Fig. 11). The ultimate strength predicted by Eqs. (9a) and (9b) was reasonably conservative in comparison with the test results except for two sections that failed in the flexural-torsional mode about the symmetric axis, as shown in Fig. 5(h). The compressive strength of thermal studs predicted by Eqs. (9a) and (9b) was more conservative than that of folded lipped channel sections with perforations in the web. For sections of 200 mm in slit length, the predicted strength was fairly conservative in comparison with test results. This may be because long slits significantly reduced local buckling stress. However, given the difficulty in predicting the strength of thermal studs, the results suggests that the proposed strength formulae for the direct strength method is suitable for predicting the ultimate strength of thermal studs.

Table 6 summarizes the results for the buckling and maximum stress of Type A and Type B sections that were longer than 1,155 mm and failed in the distortional buckling mode. There was little difference in local buckling stress between numerical and test results. Here, because local buckling stress was much lower than yield stress, there was elastic local buckling before distortional buckling in the test. However, the distortional buckling stress obtained by the buckling analysis program BAP (Ver. 2) was much higher than test results because local buckling had a negative effect on distortional buckling in the test and the interaction between local buckling and distortional buckling could not be accounted for in the buckling analysis. The material inelasticity and initial imperfections could not be sufficiently accounted for in the buckling analysis. The ultimate strength predicted by the direct strength method (DSM) was fairly conservative in comparison with the experimental maximum stress. However, the proposed strength equations with the concept of equivalent thickness should be calibrated against additional test results for their practical application. The predicted strength was too more conservative for test sections of 1,155 mm in length than for other sections in comparison with test results.

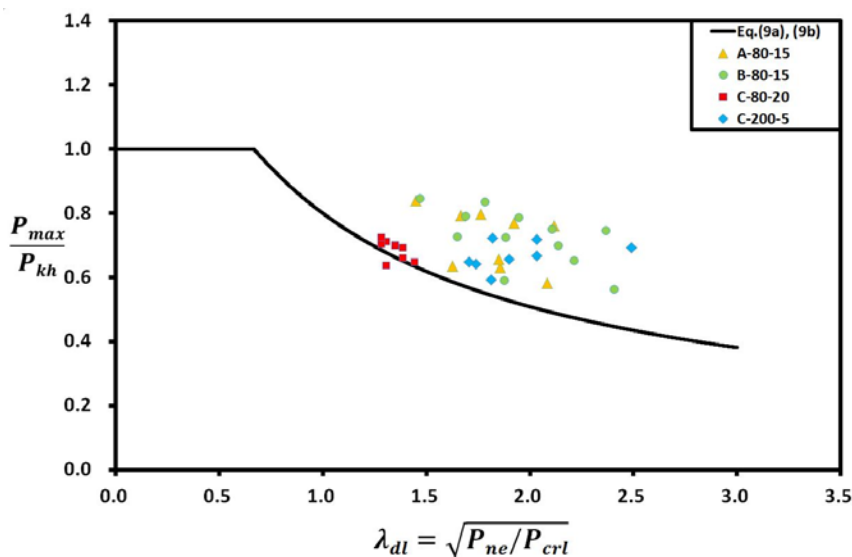


Fig. 11 Comparison of proposed DSM strength curve and test results

Table 6 Comparison of buckling and maximum stress for thermal studs

Specimens	Local buckling (MPa)		Distortional buckling (MPa)		Maximum stress (MPa)		
	Test	Analysis	Test	Analysis	Test	DSM	Test/DSM
A-80-15-1.0-1155	26.8	28.0	93.2	132.5	109.6	70.1	1.56
A-80-15-1.0-1440	25.8	28.0	67.6	140.3	78.0	71.3	1.09
A-80-15-1.2-2010	26.2	28.0	66.8	98.8	80.4	63.7	1.26
A-80-15-1.2-1155	36.3	38.4	112.8	165.9	130.8	84.0	1.55
A-80-15-1.2-1440	34.2	38.4	80.3	155.0	96.7	82.3	1.17
A-80-15-1.4-2010	35.6	38.4	66.2	97.6	83.6	70.8	1.18
A-80-15-1.4-1155	46.2	49.4	135.4	189.7	140.9	95.5	1.47
A-80-15-1.4-1440	48.3	49.4	86.4	160.2	111.0	90.7	1.22
A-80-15-1.6-2010	47.7	49.4	73.5	94.8	82.8	76.4	1.08
A-80-15-1.6-1155	57.6	60.9	135.8	204.0	150.6	104.9	1.43
A-80-15-1.6-1440	55.3	60.9	97.3	160.5	134.2	97.5	1.37
A-80-15-1.6-2010	54.3	60.9	87.5	91.5	107.4	81.0	1.32
B-80-15-1.0-1155	27.3	27.2	101.2	129.5	113.7	68.9	1.65
B-80-15-1.0-1440	24.5	27.2	80.4	138.6	88.6	70.3	1.25
B-80-15-1.0-2010	23.8	27.2	76.8	98.8	87.0	63.1	1.37
B-80-15-1.2-1155	35.7	37.4	100.4	163.2	119.3	82.8	1.44
B-80-15-1.2-1440	33.5	37.4	91.3	154.1	124.6	81.4	1.53
B-80-15-1.2-2010	31.8	37.4	80.5	97.8	96.0	70.3	1.36
B-80-15-1.4-1155	46.2	48.0	115.4	187.5	143.1	94.2	1.51
B-80-15-1.4-1440	42.2	48.0	84.3	160.0	99.8	89.8	1.11
B-80-15-1.4-2010	43.5	48.0	80.3	95.2	95.0	75.8	1.25
B-80-15-1.6-1155	53.2	59.4	129.5	202.6	157.3	103.8	1.51
B-80-15-1.6-1440	50.5	59.4	96.6	160.7	133.8	96.7	1.38
B-80-15-1.6-2010	50.1	59.4	90.4	92.0	115.7	80.5	1.34
C-200-5-1.0-410	17.8	29.6	115.7	191.6	127.2	80.0	1.59
C-200-5-1.0-820	13.7	29.6	53.3	83.7	133.8	44.8	1.42
C-200-5-1.0-1130	12.8	29.6	44.9	64.6	107.7	41.0	1.24
C-200-5-1.0-1435	15.0	29.6	39.0	54.5	128.2	38.7	1.09
C-80-20-1.0-400	76.8	100.6	127.2	258.8	135.9	123.4	1.02
C-80-20-1.0-840-1	70.7	100.6	122.0	214.0	133.8	116.9	1.06
C-80-20-1.0-840-2	72.5	100.6	92.3	214.0	127.7	116.9	1.01
C-80-20-1.0-1140-1	70.1	100.6	113.2	190.0	128.2	112.8	1.05
C-80-20-1.0-1140-2	64.1	100.6	123.7	190.0	127.9	112.8	1.05
C-80-20-1.0-1440-1	68.6	100.6	118.5	165.2	122.0	108.0	1.05
C-80-20-1.0-1440-2	69.5	100.6	92.3	165.2	109.3	108.0	0.94
C-80-20-1.0-1740-1	60.4	100.6	108.7	153.1	116.4	105.4	1.03
C-80-20-1.0-1740-2	54.9	100.6	109.4	153.1	119.9	105.4	1.06

6. Conclusions

A series of compression tests was conducted for three types of thermal studs to examine the structural behavior and performance of cold-formed steel thermal studs. The main test parameters were the number of slit lines, the slit length, and the solid distance of between adjacent slits in the longitudinal direction. Based on test results, the direct strength method was applied to thermal studs by substituting solid studs of equivalent thickness for thermal studs.

Perforations in the web of thermal studs significantly reduced the ultimate strength of solid sections according to the geometry of slits. Within a certain limit, the slit length had little effect on the buckling and ultimate strength of thermal studs. When the slit length increased, there was a slight decrease in the ultimate compressive strength. However, when the slit length exceeded 80 mm, local buckling stress was decreased linearly according to the increase in the slit length. The solid distance between slits in the longitudinal direction had little effect on the compressive strength of thermal studs. The local buckling mode of thermal studs was different from the conventional local buckling mode of plain channel sections. Solid parts between slits buckled locally first, and there was a significant post-local-buckling strength before a distortional or flexural-torsional failure. The solid section of the concept of equivalent thickness (Salhab and Wang 2008) was slightly modified, and the DSM was applied to predict the strength of thermal studs. The compressive strength of solid sections of equivalent thickness in perforated elements was reasonably predicted by the DSM relative to test results. However, the proposed method should be further verified and calibrated by using additional with various test results for its practical application.

Acknowledgments

This paper is part of a project entitled “Development of Direct Strength Method for Cold-Formed Steel Sections” conducted in the Department of Civil Engineering at the Yeungnam University, Korea. This research was supported by the 2012 research grant from the Yeungnam University.

References

- American Iron and Steel Institute (AISI) (2004), Standard, Supplement 2004 to the North American Specifications for Design of Cold-Formed Steel Structural Members, Washington D.C., USA.
- American Iron and Steel Institute Standard (AISI) (2012), North American Specifications for the Design of Cold-Formed Steel Structural Members, Washington D.C., USA.
- Cheng, B. and Li, C. (2012), “Buckling behavior of strengthened perforated plates under shear loading”, *Steel Compos. Struct., Int. J.*, **13**(4), 367-382.
- Davis, J.M., Leach, P. and Taylor, A. (1997), “The design of perforated cold-formed steel sections Subjected to axial load and bending”, *Thin-Wall. Struct.*, **29**(1-4), 41-57.
- European Committee for Standardization (ECS) (2001), Eurocode 3: Design of Steel Structures, Part 1-3: General rules- Supplementary rules for cold-formed thin gauge members and sheeting, Brussels, Belgium.
- European Committee for Standardization (ECS) (2003), Eurocode 3: Design of Steel Structures, Part 1-1: General rules and rules for buildings, Brussels, Belgium.
- FEA Co., Ltd. (2012), Lusas Element Reference Manual & User’s Manual (version 14.7).
- Hancock, G.J., Murray, T.M. and Ellifritt, D.S. (2004), *Cold-Formed Steel Structures to the AISI*

- Specification*, Marcel Dekker, Inc., NY, USA.
- Hoglund, T. and Burstand, H. (1998), "Slotted steel studs to reduce thermal bridges in insulated walls", *Thin-Wall. Struct.*, **32**(1-3), 81-109.
- Kesti, J. (2000), "Local and distortional buckling of perforated steel wall studs", Ph.D. Thesis, Helsinki University of Technology, Finland.
- Korean Standard Association (2006), KSD3506, Hot-Dip Zinc Coated Steel Sheets and Coils, Seoul, Korea. [In Korean]
- Kwon, Y.B. (2000), Buckling Analysis Program (BAP) User's Manual (Ver 2.0), Department of Civil Engineering, Yeungnam University, Korea.
- Kwon, Y.B., Kim B.S. and Hancock G.J. (2009), "Compression tests of high strength cold-formed steel channels with buckling interaction", *J. Construct. Steel Res.*, **65**(2), 278-289.
- Kwon, Y.B. and Hancock, G.J. (1992), "Post-buckling behaviour of thin-walled sections undergoing local and distortional buckling", *Comput. Struct.*, **49**(3), 507-516.
- Moen, C.D. and Schafer, B.W. (2009), "Elastic buckling of thin plates with holes in compression or bending", *Thin-Wall. Struct.*, **47**(12), 1597-1607.
- Salmi, P. (1998), Design of web-perforated steel wall studs, Fourth Finnish steel structures R&D days, Lappeenranta, Finland.
- Salhab, B. and Wang, Y.C. (2008), "Effective thickness of cold-formed thin-walled channel sections with perforated webs under compression", *Thin-Wall. Struct.*, **46**(7), 823-838.
- Schafer, B.W. (2008), "The direct strength method of cold-formed steel member design", *J. Construct. Steel Res.*, **64**(7), 766-778.
- Schafer, B.W. and Pekoz, T. (1998), *Direct Strength Prediction of Cold-Formed Steel Members using Numerical Elastic Buckling Solutions*, Thin-Walled Structures, Research and Development, (Eds. Shanmugan, N.E., Liew, J.Y.R. and Thevendran, V.), Elsevier, pp. 137-144.
- Standard Australia (2005), Cold-Formed Steel Structures AS/NZS 4600, Sydney, Australia.
- Venkataramaiah, K.R. and Roorda, J. (1982), "Analysis of local plate buckling experimental data", *Proceedings of the 6th International Specialty Conference on Cold-Formed Steel Structure*, University of Missouri-Rolla, St. Louis, MO, USA, October.
- Walker, A.C. (1975), *Design and Analysis of Cold-Formed Sections*, International Textbook Company Ltd., London, UK.
- Wang, Y.C. and Salhab, B. (2009), "Structural behavior and design of light weight structural panels using perforated cold-formed thin-walled sections under compression", *Int. J. Steel Struct.*, **9**(1), 57-67.

Nomenclature

A	Cross sectional area
b	Clear width of the plate element
b_f	Flange width
D	Web depth/slit length
F_{crl}	Elastic local buckling stress
F_{cro}	Elastic flexural/flexural-torsional buckling stress
F_{kh}	Distortional buckling limiting stress
F_{ne}	Overall column strength based on overall buckling stress
f_{nl}	Design limiting stress accounting for the interaction of local and overall buckling
F_l	Nominal strength based on local buckling stress
F_{max}	Ultimate strength determined in a test
F_y	Nominal yield stress
l	Length of the specimen
l_s	Solid distance between adjacent slits in the longitudinal direction
P_b	Total width of slits
P_{crl}	Elastic local buckling load ($= F_{crl} \times A$)
P_l	Resulting limiting load ($= F_l \times A$)
P_{nl}	Design limiting strength ($= F_{nl} \times A$)
P_{ne}	Compression member design strength ($= F_{ne} \times A$)
r	Radius of gyration
t	Plate thickness
t_f	Flange thickness
t_w	Web thickness
w_s	Distance between slits in the transverse direction
w_p	Distance between exterior slits
λ_d	Distortional buckling slenderness factor ($= \sqrt{F_y / F_{crl}}$)
λ_{nl}	Local buckling slenderness factor ($= \sqrt{F_{ne} / F_{crl}}$)
λ_{dl}	Slenderness factor ($= \sqrt{F_{kh} / F_{crl}}$)